ACS Biomaterials SCIENCE & ENGINEERING

pubs.acs.org/journal/abseba Article

Eco-Friendly Preparation of Epoxy-Rich Graphene Oxide for Wound Healing

Ying Zheng,[#] Siqiao Li,[#] Daobin Han,[#] Liangsheng Kong, Jianmin Wang, Min Zhao, Wei Cheng, Huangxian Ju, Zhongzhu Yang,* and Shijia Ding*

Cite This: *ACS Biomater. Sci. Eng.* 2021, 7, 752−763 Read Online

ACCESS | Metrics & More | Article Recommendations | Supporting Information

ABSTRACT: Despite the ever-growing endangerment caused by the multidrug resistance (MDR) of bacteria, the development of effective antibacterial materials still remains a global challenge. Current antibiotic therapies cannot simultaneously inactivate bacteria and accelerate wound healing. This study aimed to originally separate the intercalation of MnO_3^+ and the oxidation processes to synthesize epoxy-rich graphene oxide (erGO) nanofilms via an eco-friendly synthetic route, which possessed low density and large lamellar distribution and was rich in epoxide. Importantly, the MnO_3^+ could be separated from the product and recycled for preparing the next generation of erGO nanofilms, which was quite economical and eco-friendly. The erGO nanofilm was capable of successfully inhibiting Gram-negative bacteria and even had excellent growth-inhibitory effects on Gram-positive bacteria including multidrug resistance (MDR) bacteria, as evidenced by antibacterial phenomena. Additionally, the erGO nanofilm with high •C density formed from epoxide exerted excellent antibacterial effects through tight membrane wrapping and induction of lipid peroxidation. The wound-healing property of the erGO nanofilm was evaluated via treatments of wounds infected by *Staphylococcus aureus* (*S. aureus*) and *Escherichia coli* (*E. coli*), which not only killed bacteria but also accelerated wound healing in mice with a skin infection. The novel erGO nanofilm with dual antimicrobial mechanisms might serve as a promising multifunctional antimicrobial agent for medical wound dressing with high biocompatibility.

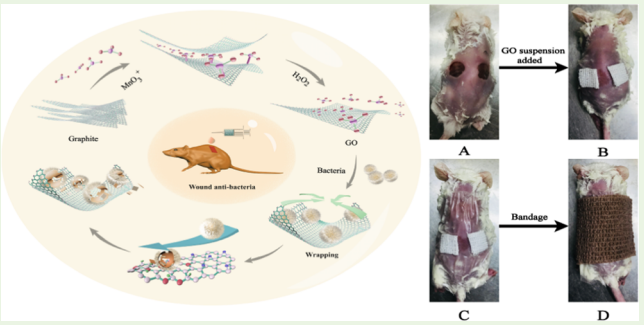

KEYWORDS: *antibacterial, eco-friendly, epoxy-rich graphene oxide, MnO_3^+ intercalation, wound dressing*

1. INTRODUCTION

The antimicrobial resistance (AMR) in bacteria, parasites, and viruses has become a global public health problem due to the widespread use of antibiotics in humans and livestock.[1] The 2016 World Health Organization report estimated that 10 million people will die per year in the next 30 years owing to AMR if nothing is done. AMR has posed a large clinical and public health burden.[2] Both acute and chronic bacterial infections in wounds may further lead to the infection of tissues, increasing morbidity and mortality.[3] Tissues infected with more than 1×10^5 bacteria per gram (or at least 1×10^6 bacteria per gram of tissue) may not show any clinical symptoms, but wound healing is seriously affected.[4] Moreover, it is difficult to control bacterial infection because of the poor blood flow and the presence of dead tissues.[5,6] Meanwhile, broad-spectrum antibiotics are still relatively scarce, and the effectiveness of antibiotics also needs to be strengthened. Therefore, global efforts to exploit nonresistant alternatives and use more effective antibacterial strategies are highly required.[7]

Consistent efforts have been made toward treating bacterial infections, as reflected by sustained and extensive developments of antibacterial materials, including nanomaterials,[8] antimicrobial peptides,[9] and cationic polymers.[10] Ideal clinical antibacterial materials should be broad-spectrum, efficient, and less cytotoxic to human cells.[11] The rapid development of nanotechnology in the field of medicine may provide a potential alternative to overcome AMR due to the structures, high antibacterial efficiency, and biosafety of nanomaterials. To date, a variety of nanomaterials, including silver nanoparticles (Ag NPs),[12] TiO_2 NPs,[13] ZnO NPs,[14] MgO NPs,[15] and graphene materials (GMs),[16] have been widely used in medical fields, which not only protect against bacteria causing morphological changes in membranes but also enhance antibacterial activities of antibiotics. Among these, Ag NPs are the most extensively adopted nanomaterials due to their excellent antibacterial properties.[17−20] However, the applica-

Received: November 11, 2020
Accepted: January 15, 2021
Published: January 25, 2021

https://dx.doi.org/10.1021/acsbiomaterials.0c01598
ACS Biomater. Sci. Eng. 2021, 7, 752−763

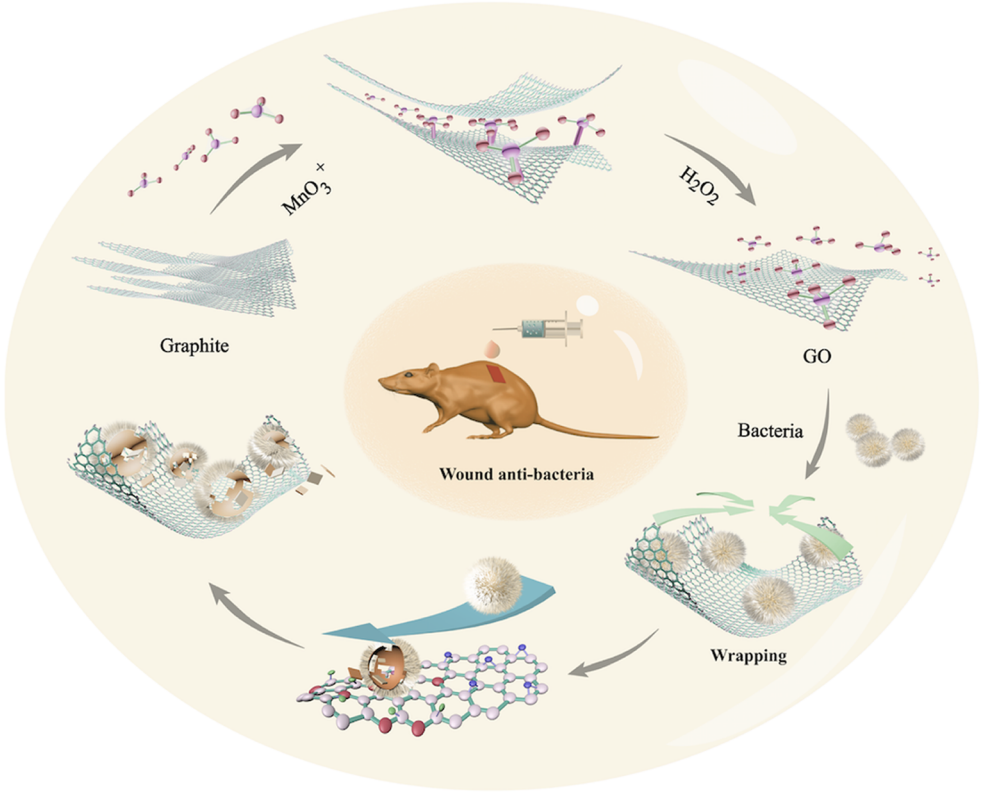

Figure 1. Schematic illustration of the erGO nanofilm for rapid sterilization and wound healing.

tion of Ag NPs as antibacterial agents is restricted because of their cytotoxicity and drug resistance.[21] Since the successful fabrication of GMs, they have attracted tremendous attention owing to their high antibacterial efficiency and low cytotoxicity.[22−24] A large number of studies showed that four types of graphene-based materials, including graphite (Gt), graphite oxide (GtO), graphene oxide (GO), and reduced graphene oxide (rGO) nanofilms, have excellent antibacterial activities.[24]

Among GMs, GO nanofilms are important materials characterized by abundant oxygen-containing groups, including epoxide, hydroxyl, and carboxyl functional groups.[25−28] These oxygen-containing groups make GO nanofilms advantageous compared with graphene in terms of the tunability in both structure and properties via a chemical reaction.[29] One of the most pressing issues for the technological application of GO nanofilms is the complexity of the synthetic process. Traditional methods mainly include Brodie,[30,31] Staudenmaier,[32,33] and Hummers methods.[34,35] The main shortcomings of these methods are as follows: (1) For the Brodie method, the synthetic process is dangerous, and the GO nanofilm is small and lacks oxygen-containing groups. (2) The Staudenmaier method is time-consuming, dangerous, and toxic. (3) The Hummers method has the highest oxidation degree compared with the others, which requires strict temperature control and produces a large amount of waste acid. A large number of studies have investigated the antibacterial activities of GO nanofilms, and several mechanisms have been put forward.[36−41] So far, the most widely recognized antibacterial mechanisms are as follows: (1) Sharp edges of GO nanofilms can cause the efflux of intracellular substances.[36] (2) Oxidative stress mediated with/without reactive oxygen species (ROS) may impact cellular functions, even leading to cell death.[39] (3) A dense GO nanofilm encapsulates bacteria and hinders the uptake of nutrients.[40] Therefore, a more scalable synthetic procedure needs to be identified, and a method needs to be developed that is safe and cost-effective, has a large lamellar distribution, and is rich in epoxide.

In this study, the epoxy-rich GO (erGO) nanofilm was synthesized with the intercalation of MnO_3^+ at room temperature. This method simplified the procedures, increased the contents of epoxide by separating the intercalation and oxidation processes, and avoided the decrease in lamellar size caused by potassium permanganate oxidation. The erGO nanofilm inactivated bacteria by tightly wrapping and agglomerating them. Furthermore, numerous $^{\bullet}C$ radicals formed from epoxide endowed the erGO nanofilm with excellent antibacterial activities by inducing lipid peroxidation. Detailed characterization of antibacterial phenomena revealed that erGO nanofilms could successfully inhibit Gram-negative and Gram-positive bacteria. Moreover, erGO nanofilms even had an excellent growth-inhibitory effect on the coccus of multidrug resistance (MDR) bacteria. The erGO nanofilm exhibited fairly low cytotoxicity and high biocompatibility even at high concentrations. The erGO nanofilm was used to treat wounds in mice infected by *Staphylococcus aureus* and *Escherichia coli* so as to explore its potential applications. It was found that the erGO nanofilm not only killed bacteria but also accelerated wound healing, suggesting the potential of the erGO nanofilm as a medical wound dressing for antibacterial application (Figure 1).

2. RESULTS AND DISCUSSION

2.1. Synthesis of a Uniform erGO Nanofilm. A large number of studies showed that GO with a larger area could wrap more bacteria, and more epoxy functional groups on the

https://dx.doi.org/10.1021/acsbiomaterials.0c01598
ACS Biomater. Sci. Eng. 2021, 7, 752−763

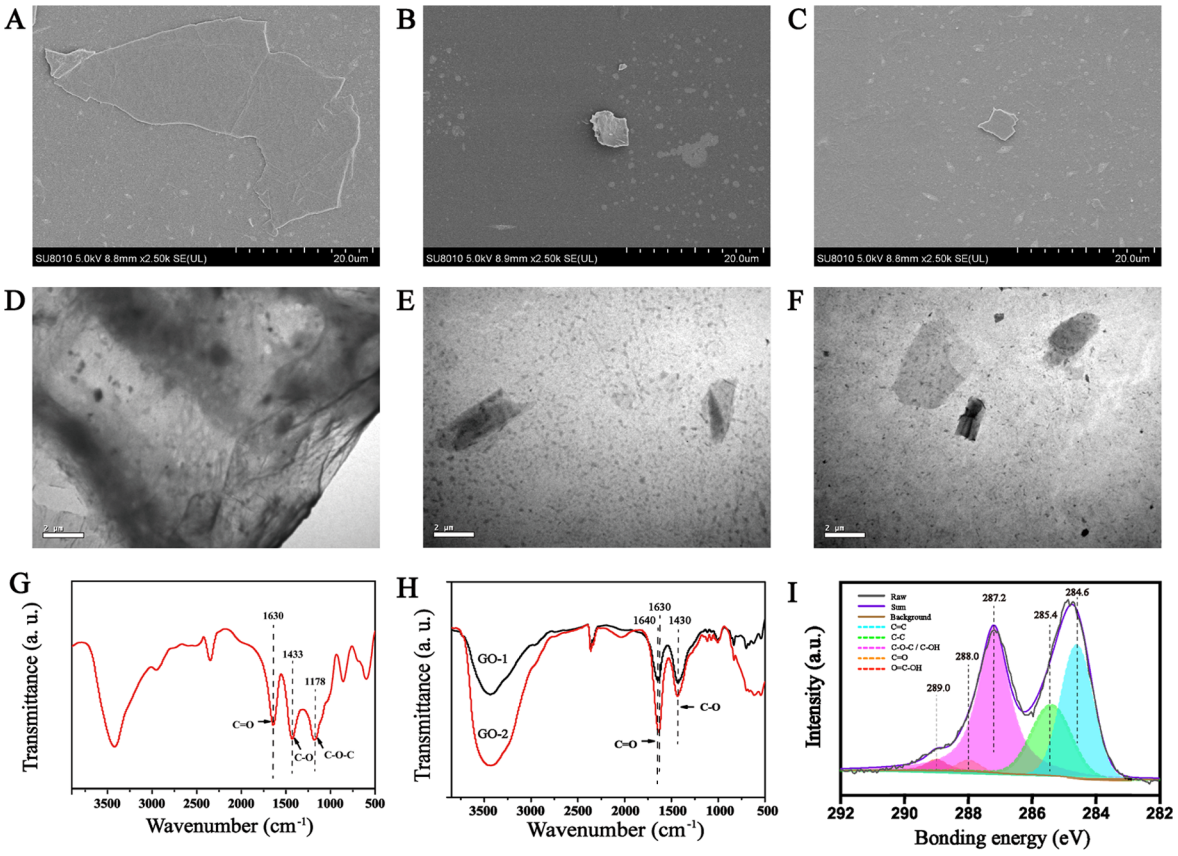

Figure 2. (A) SEM micrograph of the erGO nanofilm deposited on copper grids. (B) SEM micrograph of the control group of GO-1. (C) SEM micrograph of the control group of GO-2. (D) TEM image of the erGO nanofilm. (E) TEM image of the control group of GO-1. (F) TEM image of the control group of GO-2. (G) FTIR spectrum of functional groups on the surface of the erGO nanofilm. (H) FTIR spectrum of functional groups of the control groups of GO-1 and GO-2. (I) C1s XPS spectra of carbon and oxygen groups on the erGO nanofilm surface. Different peaks corresponded to different functional groups, and the C/O was 1.61.

base surface generated more free radicals to inhibit the growth of bacteria. However, synthesizing GO with a large area and rich in epoxy functional groups by the Hummers method is challenging because $KMnO_4$ inevitably breaks the C=C bond on the base surface, resulting in a smaller lamellar area. Therefore, the content of $KMnO_4$ in the intercalation process must be strictly controlled to avoid the occurrence of an oxidation reaction (Figure S1). Therefore, MnO_3^+ was used as the only intercalation agent, and excessive sulfuric acid was used to absorb water in the intercalation process to ensure that $KMnO_4$ was always kept at a low level so as to achieve the purpose of separating the intercalation process and the oxidation process (Figures S2 and S3).

The first step was intercalation. In this process, MnO_3^+ with a 2D planar structure as the intercalating agent was reacted with the hydroxyl (-OH) group on graphene, and then the planar structure of MnO_3^+ was transformed into a tetrahedral (3D) structure of -MnO_4. A triangular MnO_3^+ spontaneously changed into a tetrahedral MnO_4^- and stretched out the tightly stacked graphene sheets (Figure S4). As the lamellas were stretched, more MnO_3^+ entered between graphene lamellas, increasing the space for subsequent MnO_3^+. The MnO_3^+ entering in the early stage was fixed in the form of MnO_4^- and could not be further intercalated. The purpose of adding small amounts of MnO_3^+ many times was to avoid the conversion of MnO_3^+ into MnO_4^- by absorbing water, thus reducing the possibility of breaking the C=C bond. In this way, enough MnO_3^+ was available for intercalation in the whole process.

The second step was placing MnO_3^+ stably for hours. This allowed free MnO_3^+ to bind to the carbon surface as much as possible. This process guaranteed that sufficient in situ MnO_2 was obtained to catalyze the formation of epoxy groups. Finally, a purple precipitate of manganese-embedded graphene was obtained because of its high density. MnO_3^+ and H_2SO_4 could be separated from the reaction system after the second step. About 45.94% of the upper MnO_3^+ could be separated from the product and recycled to prepare the next erGO nanofilm (Figure S5).

The third step was oxidation with water. Concentrated sulfuric acid gave off heat on reaction with water. Both the bound MnO_4^- and the residual free MnO_3^+ were converted into free MnO_4^- at high temperatures. Immediately, MnO_4^- reacted with carbon to form HCO_3^- and MnO_2.

The last step was oxidation with H_2O_2. H_2O_2 reacted with bicarbonate to form percarbonate. H_2CO_4 was a key active oxidant more nucleophilic than H_2O_2. The complexes of Mn (4+) and H_2CO_4 were shown to be viable epoxidation intermediates, and a usual interpretation of the mechanism was that a Mn (4+) complex catalyzed the epoxidation reaction. Enough in situ MnO_2 could generate more epoxy functional groups because of the complete intercalation of MnO_3^+.

The synthesis of a uniform erGO nanofilm avoided the breaking of the C=C bond by free $KMnO_4$, resulting in the formation of GO with a large lamellar distribution and a large

https://dx.doi.org/10.1021/acsbiomaterials.0c01598
ACS Biomater. Sci. Eng. 2021, 7, 752−763

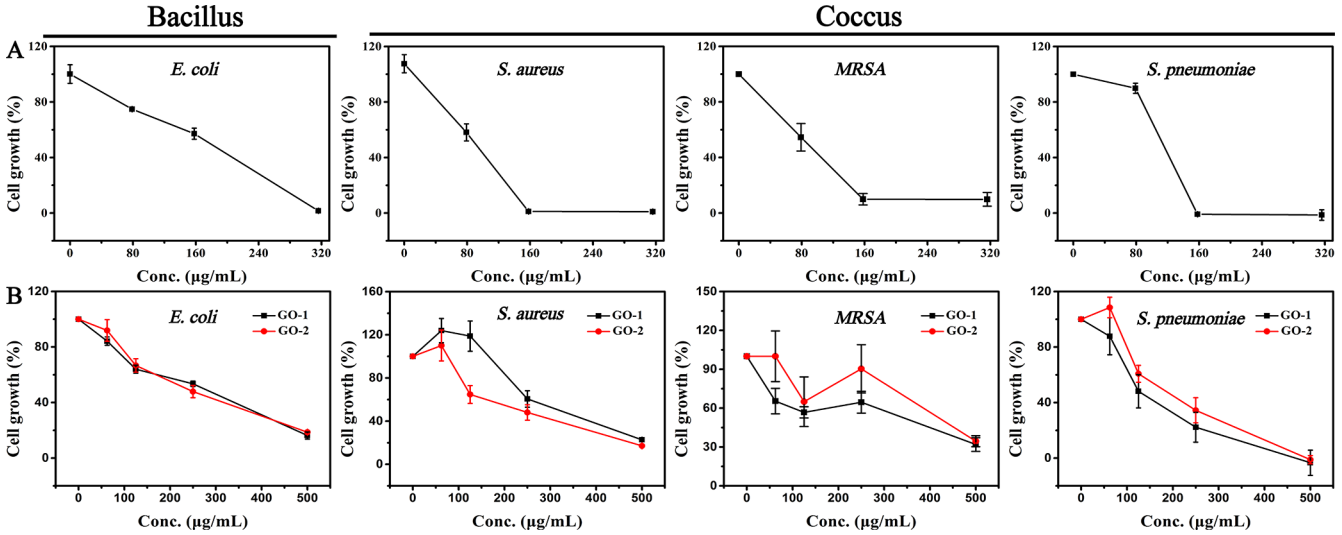

Figure 3. erGO nanofilm exhibited excellent antibacterial effects. (A) Bacterial killing effects of the erGO nanofilm (79−316 μg/mL) in *E. coli*, *S. aureus*, *MRSA*, and *S. pneumoniae* at 37 °C for 18 h. Bacterial growth was detected by measuring bacterial optical density at 600 nm. (B) Bacterial killing effects in the erGO nanofilm control groups (62.5−500 μg/mL GO-1 or GO-2) at 37 °C for 18 h. Bacterial growth was detected by measuring bacterial optical density at 600 nm.

number of epoxy groups. It was also because the base surface was kept intact, and the freeze-dried sample had a golden metallic luster. Additionally, there is no Mn bonded to the erGO nanofilm (Figure S6). More importantly, waste acid treatment was not needed, making the method quite economical and eco-friendly. The prepared erGO nanofilm was still golden after vacuum freeze-drying, which was quite different from any other GO (Figure S7).

2.2. Characterization of the erGO Nanofilm. Representative scanning electron microscopy (SEM) images (Figure 2A) showed a crystalline structure containing several layers and having the primary size of 40−60 μm. As shown in Figure 2B,C, the images demonstrated that the erGO nanofilm had large lamellae, while the primary sizes of control groups of GO were only about 3−4 μm. Transmission electron microscopy (TEM) image (Figure 2D) further showed the lamellar structure of the erGO nanofilm. The TEM images demonstrated that the erGO nanofilm had a wrinkled morphology and rougher surface than that of the control groups (Figures 2E,F). Additionally, the characteristic structures of carbonyl (1630 cm^{-1}), hydroxyl (1430 cm^{-1}), and epoxy (1178 cm^{-1}) groups of the erGO nanofilm were observed using Fourier transform infrared spectroscopy (FTIR) (Figure 2G). The FTIR spectra of the epoxy functional group of the control groups (GO-1 and GO-2) were found at significantly lower values than that of the erGO nanofilm (Figure 2H). The distribution of carbon-related groups on the erGO nanofilm was further characterized by high-resolution x-ray photoelectron spectroscopy (XPS) analysis, showing the ratio of C (58.51%) to O (36.29%) (C/O, 1.61) calculated using XPSPEAK 4.1 software. Typical bands of the binding energy of erGO at 284.6 and 285.4 eV for C═C and C−C bonds, those at 287.2 and 288 eV for C−O−C, C−OH, and C═O bonds, and those at 289 eV for O═C−OH bands were observed (Figure 2I). The binding energies of control groups at 284.6 and 285.4 eV for C═C and C−C bonds and those at 286.9 and 288.3 eV for C−O−C, C−OH, and C═O bonds were observed (Figure S8). The binding energy of C−O of erGO was 0.3 eV more than that of the control groups, showing that the C−O−C group of the erGO nanofilm was higher than that of the control groups. To accurately observe the erGO nanofilm, an atomic force microscope (AFM) was utilized to reveal an average lamella height of 1.131 nm (Figure S9), while the size of the control groups of GO was much smaller than that of the erGO nanofilm (Figure S10), further confirming the single-layer structure of the erGO nanofilm.

2.3. In Vitro Antibacterial Effects of the erGO Nanofilm. Antibacterial effects of the erGO nanofilm were evaluated against *E. coli*, *S. aureus*, Methicillin-resistant *Staphylococcus aureus* (*MRSA*), and *Streptococcus pneumoniae* (*S. pneumoniae*) as representative Gram-negative and Gram-positive bacteria, respectively. A series of erGO nanofilms (316, 158, and 79 μg/mL) were incubated with bacterial suspensions (~10^6 CFU/mL) for 18 h at 37 °C. Figure 3A shows that the viability of *E. coli* decreased to 56.94% after incubating with the erGO nanofilm (158 μg/mL) for 18 h. Meanwhile, the antibacterial activities of the erGO nanofilm in *S. aureus* were significantly higher than those in *E. coli*, suggesting excellent antimicrobial activities against *S. aureus* (97.35% killing at 158 μg/mL) and *S. aureus* (1) (99.69% killing at 158 μg/mL) (Figure S11A). Since *MRSA* is resistant to several antibiotics such as penicillin and amoxicillin, the ability of the erGO nanofilm to disinfect *MRSA* was crucial. As shown in Figure 3A, almost 90.07% of *MRSA* was killed when the concentration of the erGO nanofilm was 158 μg/mL. Hence, it was explored whether the erGO nanofilm had excellent antimicrobial activities for *Staphylococcus* only or for other cocci too. Therefore, *S. pneumoniae* was selected as a representative of *Streptococcus*. As shown in Figure 3A, the erGO nanofilm could kill about 99.99% of *S. pneumoniae* at 158 μg/mL. These results clearly demonstrated that the erGO nanofilm had preferable antibacterial effects on the coccus. The erGO nanofilm exhibited brilliant antibacterial effects on the coccus of Gram-positive bacteria. However, the control group A (GO-1) achieved only 36.00% killing in *E. coli* cells at 125 μg/mL, and 39.42% killing in *S. aureus*, 47.67% killing in *S. aureus* (1), 35.46% killing in *MRSA*, and 77.78% killing in *S. pneumoniae* at 250 μg/mL (Figure 3B). The control group B

https://dx.doi.org/10.1021/acsbiomaterials.0c01598
ACS Biomater. Sci. Eng. 2021, 7, 752−763

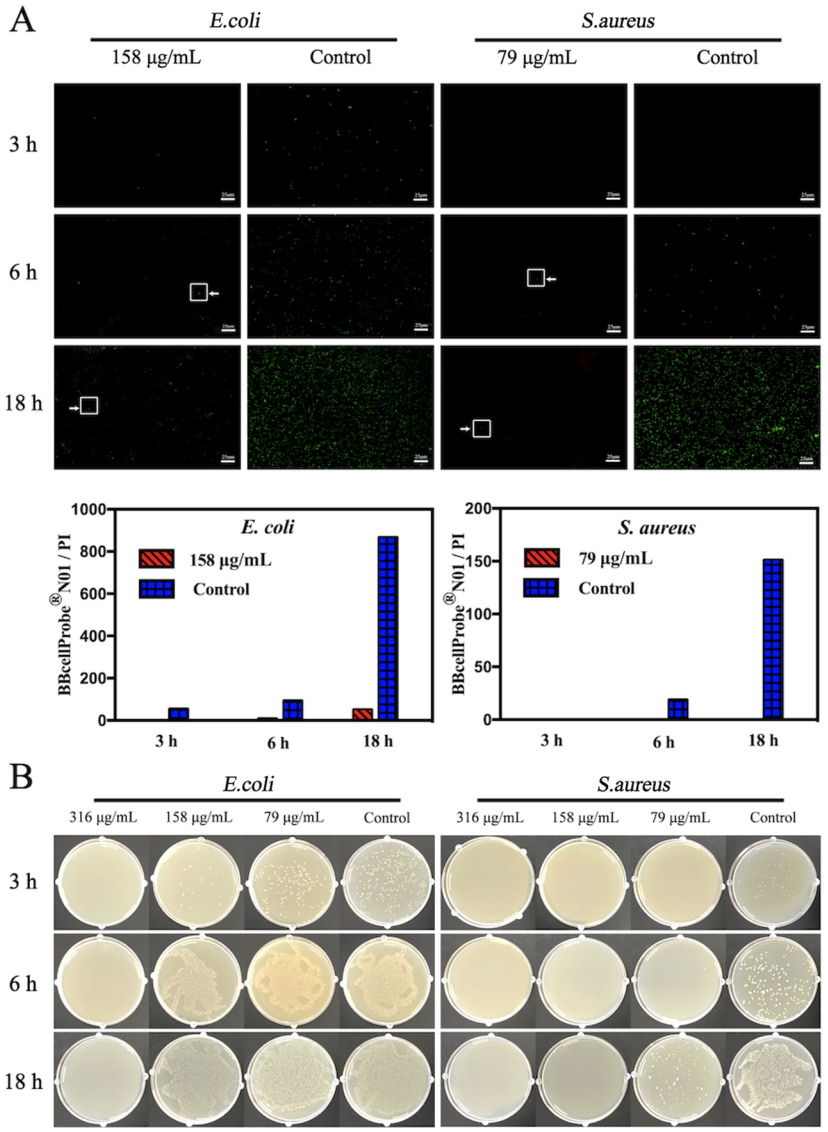

Figure 4. (A) Time gradient fluorescence images of *E. coli* and *S. aureus* after interacting with the erGO nanofilm. BBcellProbe N01 and PI were used to stain live and dead bacteria, respectively. The scale bar is 25 μm. (B) Time gradient photographs of *E. coli* and *S. aureus* colonies on agar culture plates after incubation with different concentrations of the erGO nanofilm.

(GO-2) achieved only 33.34% killing in *E. coli* cells at 125 μg/mL, and 51.95% killing in *S. aureus*, 45.40% killing in *S. aureus* (1) (Figure S11B), 10.69% killing in *MRSA*, and 65.66% killing in *S. pneumoniae* at 250 μg/mL (Figure 3B). These remarkable antibacterial results indicated that the killing efficiency of the reported erGO nanofilm for bacteria was better than those in the control groups. In addition, the antimicrobial performance of the erGO nanofilm was better than that of the other nanomaterials (Table S1).

2.4. Critical Antibacterial Mechanism of the erGO Nanofilm. Inspired by the aforementioned remarkable findings, this study focused on the mechanisms underlying the antibacterial effects of the erGO nanofilm.

A live/dead staining kit was used to visualize the bactericidal effects of the erGO nanofilm using a fluorescence microscope so as to explore the interaction between the erGO nanofilm and bacteria. As shown in Figure 4A, the bacteria showed a time-dependent (after 3, 6, and 18 h of incubation) increase in quantity in the control group without the erGO nanofilm. Minimal death was reported in the test and control groups after coculturing the bacteria with the erGO nanofilm for 18 h, as evidenced by the intense red fluorescence of intracellular propidium iodide (PI) and green fluorescence of intracellular BBcellProbe N01 binding with nucleic acids.[42] Meanwhile, the colony count corresponded to the fluorescence results (Figure 4A). As shown in Figure 4B, *E. coli* and *S. aureus* cells cultured in 96-well plates were collected, serially diluted, and transformed into Luria−Bertani (LB) agar plates to assess the number of colony-forming units after 3, 6, and 18 h of incubation. The number of colonies corresponded with the antibacterial curves. The large erGO nanofilms had a stronger interaction with bacteria to isolate bacteria from the surrounding environment but they were still alive. Although bacteria were still alive, they starved and could not form colonies in large numbers. Therefore, the red fluorescence signals of PI and green fluorescent signals of BBcellProbe N01 were less than the control group without erGO. Using these models, the results demonstrated that the erGO nanofilm exhibited superior antibacterial effects in all selected bacterial

https://dx.doi.org/10.1021/acsbiomaterials.0c01598
ACS Biomater. Sci. Eng. 2021, 7, 752−763

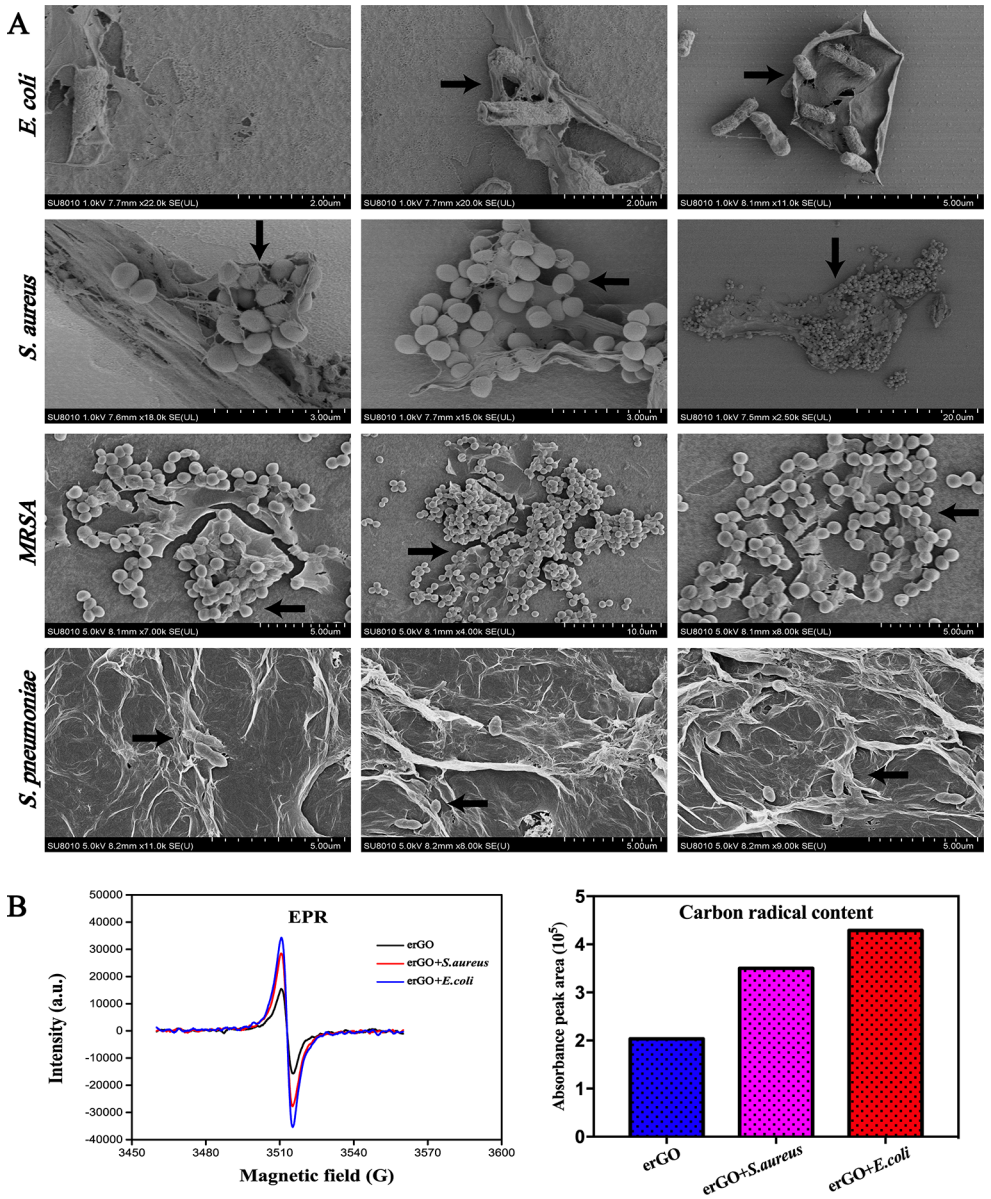

Figure 5. (A) SEM images of the changes in the morphology of *E. coli*, *S. aureus*, *MRSA*, and *S. pneumoniae* after incubation with the erGO nanofilm for 18 h. (B) Detection of $^{\bullet}$C on the erGO nanofilm surface after incubation with *E. coli* and *S. aureus* by electron paramagnetic resonance (EPR).

strains, especially the coccus of Gram-positive bacteria, compared with the control groups.

SEM images were used to study the antibacterial effects after coculturing the bacteria with GO. The *S. aureus* and *MRSA* were gathered and wrapped with the erGO nanofilm and subsequently formed huge agglomerates after exposure to 158 μg/mL GO suspension in LB medium for 18 h, as shown in Figure 5A. Further analysis of the interaction between the erGO nanofilm and *S. pneumoniae* suggested that most of the erGO nanofilms associated with the cells, and fewer bacterial membranes were damaged (Figure 5A). However, the erGO nanofilm also exhibited wrapping effects on *E. coli*, but its wrapping and agglomeration effects were far less than that on the coccus (Figure 5A). SEM images revealed that the erGO nanofilm interacted with the four types of bacterial membranes without severely damaging the bacterial membranes. Surprisingly, the wrapping performances of the erGO nanofilm were more effective than its damaging activities against bacteria. The large erGO nanofilm might have a stronger interaction with the lipid bilayer of small and round cell membranes to isolate bacteria from the surrounding environment. Meanwhile, the active surfaces of the erGO nanofilm might react with unsaturated lipids to induce lipid peroxidation, generate ROS, and exert subsequent hazardous effects. Without sufficient nutrients and appropriate conditions, slow reproduction or even death of bacteria might occur, similar to other organisms. Although bacteria were still alive, they could not form bacterial colonies. Bacteria might become inactive, but they would start forming colonies once under appropriate conditions. A number of studies suggested that wrapping bacteria was the critical mechanism underlying the antibacterial activities of the erGO nanofilm, except for nano-knives and oxidative stress. The antibacterial process comprised two crucial steps: first wrapping bacteria and then agglomerating to isolate them from the outside environment so that they could

https://dx.doi.org/10.1021/acsbiomaterials.0c01598
ACS Biomater. Sci. Eng. 2021, 7, 752−763

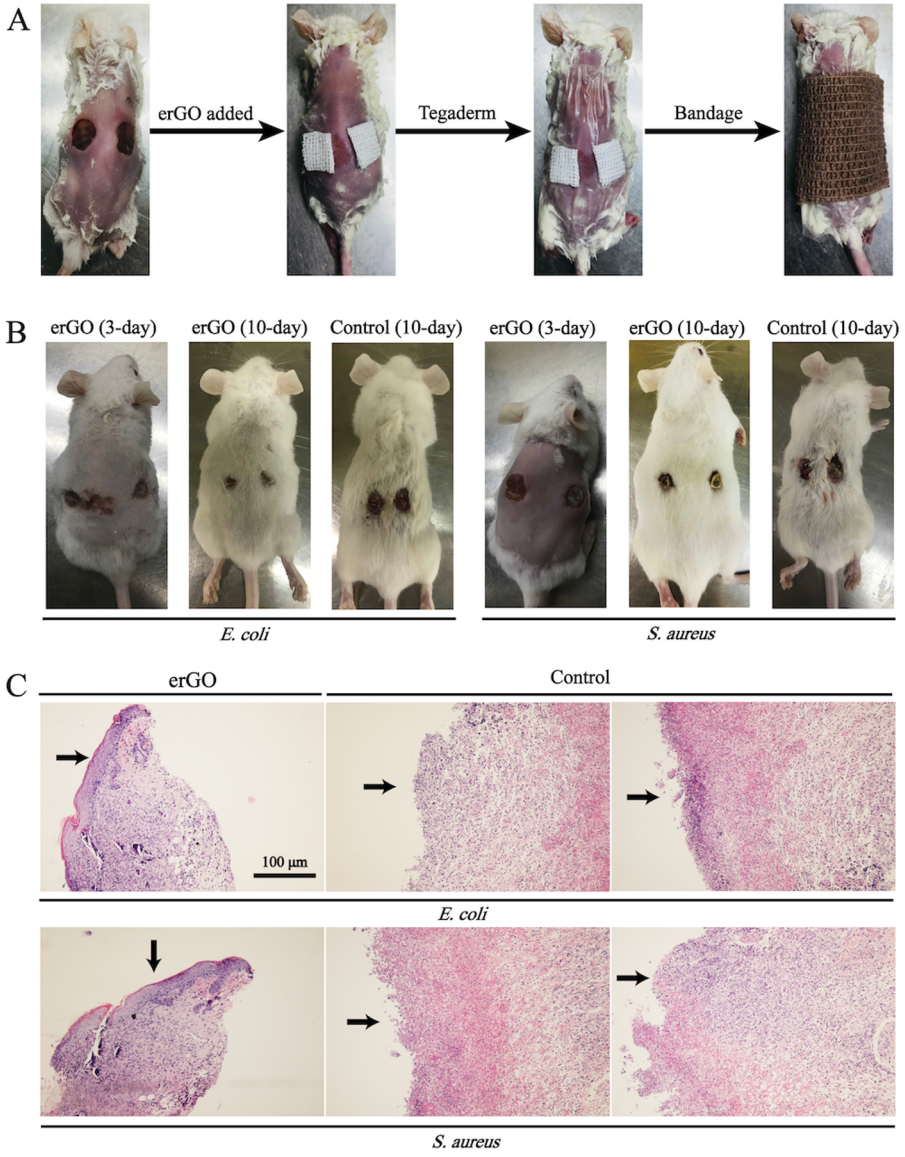

Figure 6. (A) Mice models of infectious wounds (treated with 10 μL of 1 × 10^6 CFU/mL *E. coli* and *S. aureus* and 100 μL of 158 μg/mL erGO nanofilm). (B) Photographs of *E. coli*- and *S. aureus*-infected wounds after 3- and 10-day treatments with the erGO nanofilm and an equal amount of aseptic saline water. (C) Hematoxylin and eosin staining of skin tissues in mice wounds. The scale bar is 100 μm.

not get enough nutrients. Finally, the bacteria starved and could not form colonies in large numbers.

2.5. Promotion of the Antibacterial Effects by Carbon Radicals (•C). Previous studies indicated that •C radicals were generated during the disruption of C═C bonds when graphite was treated with strong oxidants to prepare an erGO nanofilm. Meanwhile, it was possible that •C radicals could also be modulated by the oxygen-containing groups, mainly the epoxy (−COC−) group.[43] The isolated electrons in the carbon p orbitals were regularly conjugated by the π bonds, forming •C radicals on the surface of the erGO nanofilm.[44] As reported, the isolated electrons in the p orbitals of the carbon atom on the erGO nanofilm surface were located in the π-network plane, allowing them to conjugate with the π electrons of neighboring double bonds to form π-conjugated •C radicals.[44] The •C radicals could transfer from the C atom to the adjacent double bonds in the membrane, leading to the formation of the lipid peroxide radical.[45] The electron paramagnetic resonance (EPR) analysis was used to characterize the •C density on the erGO nanofilm surface after coculturing with *E. coli* and *S. aureus* strains so as to explore whether the •C radicals had any effect on the bacterial membranes. As shown in Figure 5B, the erGO nanofilm cocultured with *E. coli* showed a significantly higher EPR signal compared with the erGO nanofilm cocultured with *S. aureus*. In summary, these changes indicated that the •C radicals on the surface of the erGO nanofilm cocultured with *E. coli* were more active than those on the erGO nanofilm cocultured with *S. aureus* because the reaction degree of the −COC− group with the cellular membranes of *E. coli* was higher than that with the cellular membranes of *S. aureus*. Moreover, as shown in Figure S12, the contents of MDA of *E. coli* and *S. aureus* were 21.42 and 15.52 nmol/mL after incubating with the erGO nanofilm (158 μg/mL) for 18 h, respectively. The erGO nanofilm cocultured with *E. coli* (Figure S12A) showed a significantly higher content of MDA than the erGO nanofilm cocultured with *S. aureus* (Figure S12B) at the same concentration. These data demonstrated that the bactericidal effects of the erGO nanofilm were

https://dx.doi.org/10.1021/acsbiomaterials.0c01598
ACS Biomater. Sci. Eng. 2021, 7, 752−763

dependent on interactions with the bacterial membrane, where surface-reactive groups such as the •C could lead to membrane damage and even cell death as a result of lipid peroxidation. In summary, the critical antibacterial mechanism of the large erGO nanofilm was wrapping the lipid bilayer of small and round cell membranes to isolate bacteria from the surrounding environment. Meanwhile, the active surfaces of the erGO nanofilm could lead to lipid peroxidation to damage bacteria.

2.6. Cytotoxicity of the erGO Nanofilm. The cytotoxicity of the erGO nanofilm was evaluated by incubating it with human epithelial cells. Figure S13A shows that the cytotoxicity of the erGO nanofilm was lower than that of Au NPs; it was reported as a noncytotoxic biomaterial after 18-h incubation. In addition, no significant difference was found in cytotoxicity between these two biomaterials ($P < 0.01$). The cell viability ratios were greater than 100% at each concentration, indicating the low cytotoxicity of the erGO nanofilm even at high concentrations.

2.7. Biocompatibility of the erGO Nanofilm. The hemolysis test is the most regular method to determine the hemocompatibility of antibacterial biomaterials. The interaction of red blood cells (RBCs) with biomaterials can cause the release of hemoglobin.[46,47] In this study, the hemolytic activity of the erGO nanofilm was determined using a microplate reader at 576 nm. The hemolysis rate was less than 1% at each concentration of the erGO nanofilm after 1-h incubation at 37 °C (Figure S13B). These results demonstrated that the erGO nanofilm had excellent compatibility.

2.8. In Vivo Wound Healing. Two symmetrical full-thickness skin defects were produced on the back of each mouse and inoculated with *E. coli* and *S. aureus* (1×10^6 CFU/mL), respectively, to evaluate wound healing in vivo (Figure 6A). The erGO nanofilm was then added to cover the wounds. All mice were still active during the study; however, they showed the manifestations of bacterial infection, such as emaciation and inadequate activity.[48]

After 3 days, the wounds covered with the erGO nanofilm healed, and the mice became active again. However, the mice without the erGO nanofilm treatment were inactive and their wounds were still infected. For the wounds with the erGO nanofilm, re-epithelialization was initiated and most of the wounds already formed scabs. Nevertheless, the wounds without the erGO nanofilm were still in a state of suppurating infection (Figure 6B). Plenty of purulent secretions were observed around the wounds in the group of mice without erGO nanofilm treatment; also, the area of the wounds increased, indicating sustained wound infection. The wounds treated with the erGO nanofilm were much smaller than those not treated with the erGO nanofilm (Figure 6B). The former was still open, with purulent secretion on the 10th day, while the latter was completely scabby. The results showed that wound healing was accelerated after treatments with the erGO nanofilm.

The antimicrobial efficacy in each group was assessed depending on the number of viable *E. coli* and *S. aureus* recovered from the wounds after 10 days. The *S. aureus* and *E. coli* counts in the infected wounds of mice with or without the erGO nanofilm are shown in Figure S14. The counts of *E. coli* and *S. aureus* were 53.82 and 32.30%, respectively. The counts of viable *S. aureus* in wounds treated with the GO suspension were lower than those of *E. coli* in wounds, but the difference was not statistically significant ($P < 0.01$).

Images of hematoxylin and eosin (H&E)-stained wounds after 10 days of treatment are shown in Figure 6C. In the initial stage, the granulation tissues were loosely arranged and infiltrated by neutrophils, eosinophils, and plasma cells. Neutrophils were abundant in the wound space, suggesting an early inflammatory response of the body.[48,49] Previous studies indicated that faster angiogenesis and good distribution of fibroblasts might facilitate the growth of granulation tissues, leading to quicker and better re-epithelialization.[50−55] These histological results were consistent with the wound appearance shown in Figure 6B. All in all, the in vivo experiments in mice showed that the erGO nanofilm inhibited bacterial proliferation and promoted wound healing.

3. CONCLUSIONS

In summary, the erGO nanofilm with a large lamellar distribution and low density and rich in epoxide groups was successfully synthesized through the intercalation of MnO_3^+ without any temperature control for inactivating or killing bacteria. The waste acid treatment was not required after the preparation of the erGO nanofilm, making the process more economical and eco-friendly. Compared with the reported GO synthesis methods, the intercalation and oxidation processes were separated, ensuring the adjustments of the species and concentrations of oxygen-containing functional groups on the erGO nanofilm surface. The antibacterial tests in vitro confirmed the superior antibacterial effects of the film, inhibiting the growth of both Gram-negative and Gram-positive bacteria via wrapping, agglomeration, and •C radical formation. Moreover, the erGO nanofilms with low cytotoxicity and high biocompatibility were capable of killing bacteria and accelerating wound healing during the treatments of *S. aureus*- and *E. coli*-infected wounds. Therefore, the erGO nanofilm is expected to be a novel antibacterial and anti-inflammatory dressing with high biosafety in clinic.

4. EXPERIMENTAL SECTION

4.1. Chemicals. $KMnO_4$, H_2SO_4, $NaNO_3$, Na_2S, graphite powder, and GO nanofilms (control groups) were purchased from Sangon (Shanghai, China). The BBcellProbe N01/PI kit was purchased from BestBio (Shanghai, China). The LB broth and agar culture plates were provided by Sangon (Shanghai, China). Pentobarbital was provided by Sigma (MO)

4.2. Synthesis of the erGO Nanofilm. The erGO nanofilm was prepared by the improved Hummers method. Graphite pretreatment: 0.5 g of graphite powder, 46 mL of H_2SO_4, and 0.5 g of $NaNO_3$ were mixed for 2 h at room temperature to obtain mixture A. Preparation of MnO_3^+: $NaNO_3$ (0.5 g), 3 g of $KMnO_4$, and 46 mL of H_2SO_4 were mixed in an Erlenmeyer flask with constant shaking for 1.5 h to obtain mixture B. Further, 4 mL of mixture B was added to mixture A every 20 min for complete reaction with graphene, and then the manganese-embedded graphene was obtained using MnO_3^+. After the intercalation step, 40 mL of H_2O_2 was added to the mixture to oxidize and quench the reaction. Finally, the erGO nanofilm was successfully synthesized by this improved Hummers method at room temperature.

4.3. Characterizations of the erGO Nanofilm. The erGO nanofilm was examined using TEM, SEM, AFM, XPS, FTIR, and UV−vis absorption spectra. The GO nanofilms in the control groups were examined using TEM, SEM, AFM, FTIR, and UV−vis absorption spectra. FTIR spectroscopy (4000−500 cm^{-1}) was recorded with a Magna IR-750 spectrometer (Nicolet, USA) in transmission mode, and the data were logged as absorbance units. For TEM analysis, the sample was characterized using a G2F20 microscope (FEI, USA). The erGO nanofilm (500 μg/mL) was

https://dx.doi.org/10.1021/acsbiomaterials.0c01598
ACS Biomater. Sci. Eng. 2021, 7, 752−763

placed on copper grids. After gold coating, the sample was characterized using a GeminiSEM 300 microscope (Zeiss, Germany) at 15 kV. For AFM analysis, the erGO nanofilm was measured using a Multimode Nanoscope IIIa scanning probe microscopy system (Veeco, USA). XPS characterization was carried out on an ESCALAB 250Xi spectrometer (Thermo, USA). UV−Vis absorption spectra were recorded using a UV-2550 spectrophotometer (Shimadzu, Japan).

4.4. Microorganisms and Growth Conditions. *E. coli* ATCC 25922, *S. aureus* ATCC 25923, *S. aureus* (1) ATCC 29213, *MRSA*, and *S. pneumoniae* ATCC 49619 were used in this study. These bacterial strains were obtained from the Chongqing Center for Disease Control and Prevention. The bacteria were stored at -80 °C and resuscitated on blood plates at 37 °C for 12 h. Single colonies were grown in 7 mL of LB broth for 4−6 h at 37 °C. The bacterial suspensions were centrifuged for 3 min at 9000 rpm. After removing the supernatant, the bacteria were washed twice with PBS and then diluted to 0.5 CFU/mL (measured with a microplate reader).

4.5. Antibacterial Effects of the erGO Nanofilm In Vitro. Growth inhibition curves were constructed to evaluate the antibacterial performances of the erGO nanofilm and the controls. The erGO nanofilm was serially diluted with LB broth to obtain a series of different concentrations of the nanofilm (316, 158, and 79 μg/mL). The controls were diluted in the same way (500, 250, 125, and 62.5 μg/mL). Exponentially growing bacteria with McFarland (MCF) of 0.5 were further diluted 100 times (~10^6 CFU/mL) and used as the test inoculum. Then, 10 μL of bacteria (~10^6 CFU/mL) were inoculated in each group. After incubation at 37 °C for 18 h, the 96-well plates were detected using a SpectraMax M5 microplate reader at 600 nm. The growth curves were calculated using the following equation (eq 1)

$$\text{growth}\% = (A_{\text{GO,b}} - A_{\text{GO,l}})/(A_{\text{b}} - A_{\text{l}}) \times 100\% \quad (1)$$

where $A_{\text{GO,b}}$ represents the absorbance of the erGO nanofilm incubated with bacteria, $A_{\text{GO,l}}$ represents the absorbance of the erGO nanofilm without any bacteria, A_{b} represents the absorbance of bacteria without any material, and A_{l} is the absorbance of LB broth containing no bacteria and material.

4.6. Visualization of the erGO Nanofilm in Bacteria Using SEM. After incubating with 159 μg/mL erGO nanofilm for 18 h at 37 °C, *E. coli* and the erGO nanofilm were washed twice with aseptic PBS, followed by fixation with 2.5% glutaraldehyde in PBS for 3 h at room temperature. After drying for 3 days, the cover slides were placed on copper grids. After incubating with 79.5 μg/mL GO for 18 h at 37 °C, *S. aureus* ATCC 25923, *S. aureus* ATCC 29213, *MRSA*, and *S. pneumoniae* ATCC 49619 were tested using the aforementioned method. The samples were imaged using an SU8010 SEM at 5 kV.

4.7. EPR Spectra of the erGO Nanofilm after Incubation with Bacteria. The bacteria were cultured with 159 μg/mL erGO nanofilm for 18 h at 37 °C, and then the mixtures were washed twice with aseptic PBS. Further, the mixtures (1 mg) were dried through vacuum freeze-drying. The EPR spectra were detected with an X-band Bruker A300−10/12 spectrometer and measured at a frequency of 9.852974 GHz, attenuator at 10 dB, center field at 3510 G, attenuator at 13.0 dB, and g value at 2.0.

4.8. Content of MDA of Bacteria after Incubation with the erGO Nanofilm. The erGO nanofilm was serially diluted with LB broth to obtain a series of different concentrations of the nanofilm (316, 158, and 79 μg/mL). Exponentially growing bacteria with McFarland (MCF) of 0.5 were further diluted 100 times (~ 10^6 CFU/mL) and used as the test inoculum. Then, 10 μL of bacteria (~10^6 CFU/mL) were inoculated in each group. After incubation at 37 °C for 18 h, reagent 1, reagent 2, and reagent 3 were added sequentially, and then 96-well plates were detected using a SpectraMax M5 microplate reader at 532 nm. The contents of MDA were calculated using the following equation (eq 2)

$$\text{MDA} = (A_{\text{t}} - A_{\text{b}})/(A_{\text{c}} - A_{\text{b}}) \times 10 \quad (2)$$

where A_{t} represents the absorbance of the erGO nanofilm incubated with bacteria, A_{c} represents the absorbance of the standards, and A_{b} is the absorbance of the blank control group.

4.9. Fluorescence Images of *E. coli* and *S. aureus*. The fluorescence images were obtained using a BBcellProbe N01/PI staining kit. The green fluorescence probe BBcellProbe N01 with membrane permeability selectively bound to DNA after entering the bacteria. The fluorescence intensity of the probe was weak before it entered the cell membrane. When BBcellProbe N01/PI bound to DNA, its fluorescence intensity increased greatly. PI could not penetrate the membrane of living bacteria, and hence only stained the dead bacterial cells. After incubation with the erGO nanofilm for 3, 6, or 18 h, 100 μL of suspensions were collected in 1.5 mL Eppendorf tubes. The growing bacteria were subjected to 10-fold serial dilutions with 900 μL of PBS. The bacteria were stained with BBcellProbe N01 and PI for 20 min and were observed under a microscope.

4.10. Hemolysis Assay. Fresh human RBCs were diluted with sterile Dulbecco's phosphate-buffered saline (DPBS) to obtain a stock suspension of RBCs (4 vol% blood cells). For the hemolytic activity of the erGO nanofilm, 100 μL of RBC suspensions were mixed with 100 μL of the erGO nanofilm (ranging from 316 to 79 μg/mL in serial twofold dilutions with PBS) in a 96-well plate. After incubation at 37 °C for 1 h, the optical density (OD) of the mixtures was recorded at 576 nm. The control group containing only PBS was used as a reference for 0% hemolysis. The absorbance of RBCs cultured with Ag NPs was taken as 100% hemolysis. The hemolysis by the erGO nanofilm was determined using the following equation (eq 3)

$$\text{hemolysis}\% = (A_{\text{GO,R}} - A_{\text{p}})/(A_{\text{Ag}} - A_{\text{p}}) \times 100\% \quad (3)$$

where $A_{\text{GO, R}}$ represents the absorbance of incubation with RBCs and the ErGO nanofilm, A_{Ag} represents the absorbance of incubation with RBCs and Ag NPs, and A_{p} indicates the absorbance of PBS containing no RBCs and material.

4.11. Cytotoxicity Assay. The cytotoxicity of the erGO nanofilm was evaluated using human epithelial cells. For the cytotoxicity activity of the erGO nanofilm, about 5×10^3 of the human epithelial cells were mixed with 100 μL of the erGO nanofilm (ranging from 316 to 79 μg/mL in serial twofold dilutions with PBS) in a 96-well plate. After incubation at 37 °C for 24 h, the OD of the mixtures was recorded at 450 nm. The absorbance of the human epithelial cells cultured with Au NPs was taken as the control for 0% cytotoxicity. The cytotoxicity of the erGO nanofilm was calculated using the following equation (eq 4)

$$\text{cytotoxicity}\% = A_{\text{GO,T}}/A_{\text{Au}} \times 100\% \quad (4)$$

where $A_{\text{GO,T}}$ represents the absorbance of incubation with the human epithelial cells and the erGO nanofilm and A_{Au} represents the absorbance of incubation with the human epithelial cells and Au NPs.

4.12. Models of *E. coli* and *S. aureus* Infection in Mice. The applications of the erGO nanofilm on mice were evaluated using *E. coli* and *S. aureus* infection modes. Twelve healthy female Kunming (KM) mice, aged 6−8 weeks, were obtained from the Experimental Animal Center of Chongqing Medical University. They were all fed under SPF standard experimental conditions. Twelve female mice were randomly divided into four groups: *E. coli* infection with the erGO nanofilm treatment group (n = 3), *E. coli* infection without any treatment group (n = 3), *S. aureus* infection with the erGO nanofilm treatment group (n = 3), and *S. aureus* infection without any treatment group (n = 3). Anesthesia was performed by injecting 3% pentobarbital (30 mg/kg body weight) into the abdominal cavity. A total of three mice were used in each group. Then, the back hair of mice was shaved completely with a razor and 7% Na_2S. Two full-thickness wounds on the back of mice were made with a 7-mm skin biopsy punch. Then, 10 μL of 1×10^6 CFU/mL of *E. coli* and *S. aureus* were added to the wound. After bacterial suspensions completely penetrated into the wound, 100 μL of 158 μg/mL erGO nanofilm was administered to the experimental groups. For comparison, an equal amount of aseptic saline was administered to the

https://dx.doi.org/10.1021/acsbiomaterials.0c01598
ACS Biomater. Sci. Eng. 2021, 7, 752−763

control group. Next, cotton gauzes were placed on the wounds. The cotton gauzes were covered with Tegaderm (3M, Singapore) and finally the mice were wrapped with bandage (3M) to protect the wounds.

4.13. Bacterial Counts and Histological Analysis in Wound Tissue. After 10 days of treatments, the mice were euthanized using pentobarbital and CO_2. The wound tissues were excised and put into 1 mL of aseptic PBS. The colonies were counted by making 10-fold continuous dilutions and culturing on LB agar for 24 h at 37 °C. The wound tissues were prepared on glass slides and then stained with H&E. The images of the stained wound tissues were captured by microscopy.

■ ASSOCIATED CONTENT

Supporting Information

The Supporting Information is available free of charge at https://pubs.acs.org/doi/10.1021/acsbiomaterials.0c01598.

Comparison of antibacterial action between the erGO and other reported nanosized metals; equations of the formation of 2D planar MnO_3^+; erGO nanofilm synthesis conditions and reagent quantities; UV absorption spectrum; standard curve of MnO_3^+; UV absorption spectrum of erGO nanofilm; vacuum freeze-drying of erGO nanofilm; XPS spectrum; images (PDF)

■ AUTHOR INFORMATION

Corresponding Authors

Zhongzhu Yang − *College of Medical Technology, Chengdu University of Traditional Chinese Medicine, Chengdu 611137, China*; Phone: +86-23-68485688; Email: zzyang@cdutcm.edu.cn; Fax: +86-23-68485786

Shijia Ding − *Key Laboratory of Clinical Laboratory Diagnostics (Ministry of Education), College of Laboratory Medicine, Chongqing Medical University, Chongqing 400016, China*; orcid.org/0000-0002-9183-1656; Phone: +86-23-68485688; Email: dingshijia@163.com; Fax: +86-23-68485786

Authors

Ying Zheng − *Key Laboratory of Clinical Laboratory Diagnostics (Ministry of Education), College of Laboratory Medicine, Chongqing Medical University, Chongqing 400016, China*

Siqiao Li − *Department of Forensic Medicine, Faculty of Basic Medical Sciences, Chongqing Medical University, Chongqing 400016, China*

Daobin Han − *Key Laboratory of Clinical Laboratory Diagnostics (Ministry of Education), College of Laboratory Medicine, Chongqing Medical University, Chongqing 400016, China*

Liangsheng Kong − *Key Laboratory of Clinical Laboratory Diagnostics (Ministry of Education), College of Laboratory Medicine, Chongqing Medical University, Chongqing 400016, China*

Jianmin Wang − *Key Laboratory of Clinical Laboratory Diagnostics (Ministry of Education), College of Laboratory Medicine, Chongqing Medical University, Chongqing 400016, China*

Min Zhao − *Key Laboratory of Clinical Laboratory Diagnostics (Ministry of Education), College of Laboratory Medicine, Chongqing Medical University, Chongqing 400016, China*

Wei Cheng − *The Center for Clinical Molecular Medical detection, The First Affiliated Hospital of Chongqing Medical University, Chongqing 400016, China*; orcid.org/0000-0002-1921-9761

Huangxian Ju − *State Key Laboratory of Analytical Chemistry for Life Science, School of Chemistry and Chemical Engineering, Nanjing University, Nanjing 210023, China*; orcid.org/0000-0002-6741-5302

Complete contact information is available at: https://pubs.acs.org/10.1021/acsbiomaterials.0c01598

Author Contributions

#Y.Z., S.L., and D.H. contributed equally to this work.

Notes

The authors declare no competing financial interest.

■ ACKNOWLEDGMENTS

We are grateful to the National Natural Science Foundation of China (81873980, 81873972), the National Science and Technology Major Project of the Ministry of Science and Technology of China (2018ZX10732202), and the Chongqing Medical University Graduate Talent Training Program (BJRC201925) for financial support.

■ REFERENCES

(1) Abadía-Patiño, L.; Christiansen, K.; Bell, J.; Courvalin, P.; Périchon, B. VanE-Type Vancomycin-Resistant Enterococcus Faecalis Clinical Isolates from Australia. *Antimicb. Agents Chemother.* **2004**, *48*, 4882−4885.

(2) de Kraker, M. E. A.; Stewardson, A. J.; Harbarth, S. Will 10 Million People Die a Year Due to Antimicrobial Resistance by 2050? *PLOS Med* **2016**, *13*, No. e1002184.

(3) Haraga, I.; Nomura, S.; Fukamachi, S.; Ohjimi, H.; Hanaki, H.; Hiramatsu, K.; Nagayama, A. Emergence of Vancomycin Resistance during Therapy against Methicillin-Resistant *Staphylococcus Aureus* in a Burn Patient-Importance of Low-Level Resistance to Vancomycin. *Int. J. Infect. Dis.* **2002**, *6*, 302−308.

(4) Hiramatsu, K.; Aritaka, N.; Hanaki, H.; Kawasaki, S.; Hosoda, Y.; Hori, S.; Fukuchi, Y.; Kobayashi, I. Dissemination in Japanese Hospitals of Strains of *Staphylococcus Aureus* Heterogeneously Resistant to Vancomycin. *Lancet* **1997**, *350*, 1670−1673.

(5) Robson, M. C.; Mannari, R. J.; Smith, P. D.; Payne, W. G. Maintenance of Wound Bacterial Balance. *Am. J. Surg.* **1999**, *178*, 399−402.

(6) Robson, M. C.; Cooper, D. M.; Aslam, R.; Gould, L. J.; Harding, K. G.; Margolis, D. J.; Ochs, D. E.; Serena, T. E.; Snyder, R. J.; Steed, D. L.; Thomas, D. R.; Wiersma-Bryant, L. Guidelines for the Treatment of Venous Ulcers. *Wound Repair Regen.* **2006**, *14*, 649−662.

(7) Stadelmann, W. K.; Robson, M. C.; Greenwald, D. P. Aprotinin in Ischemia-Reperfusion injury: flap survival and neutrophil response in a rat skin flap model. *Microsurgery* **1998**, *18*, 354−361.

(8) Richter, A. P.; Brown, J. S.; Bharti, B.; Wang, A.; Gangwal, S.; Houck, K.; Cohen Hubal, E. A.; Paunov, V. N.; Stoyanov, S. D.; Velev, O. D. An Environmentally Benign Antimicrobial Nanoparticle Based on a Silver-Infused Lignin Core. *Nat. Nanotechnol.* **2015**, *10*, 817−823.

(9) Ma, Z.; Wei, D.; Yan, P.; Zhu, X.; Shan, A.; Bi, Z. Characterization of Cell Selectivity, Physiological Stability and Endotoxin Neutralization Capabilities of α-Helix-Based Peptide Amphiphiles. *Biomaterials* **2015**, *52*, 517−530.

(10) Phillips, D. J.; Harrison, J.; Richards, S.-J.; Mitchell, D. E.; Tichauer, E.; Hubbard, A. T. M.; Guy, C.; Hands-Portman, I.; Fullam, E.; Gibson, M. I. Evaluation of the Antimicrobial Activity of Cationic Polymers against Mycobacteria: Toward Antitubercular Macromolecules. *Biomacromolecules* **2017**, *18*, 1592−1599.

(11) Jain, A.; Duvvuri, L. S.; Farah, S.; Beyth, N.; Domb, A. J.; Khan, W. Antimicrobial Polymers. *Adv. Healthcare Mater.* **2014**, *3*, 1969−1985.
(12) Kumar, A.; Vemula, P. K.; Ajayan, P. M.; John, G. Silver-Nanoparticle-Embedded Antimicrobial Paints Based on Vegetable Oil. *Nat. Mater.* **2008**, *7*, 236−241.
(13) Wei, C.; Lin, W. Y.; Zaina, Z.; Smith, R. L.; Rajeshwar', K.; et al. Bactericidal Activity of Ti02 Photocatalyst in Aqueous Media: Toward a Solar-Assisted Water Disinfection System. *Environ. Sci. Technol.* **1994**, *28*, 934−938.
(14) Wagner, G.; Korenkov, V.; Judy, J.; Bertsch, P. Nanoparticles Composed of Zn and ZnO Inhibit Peronospora Tabacina Spore Germination in Vitro and P. Tabacina Infectivity on Tobacco Leaves. *Nanomaterials* **2016**, *6*, 50.
(15) Leung, Y. H.; Ng, A. M. C.; Xu, X.; Shen, Z.; Gethings, L. A.; Wong, M. T.; Chan, C. M. N.; Guo, M. Y.; Ng, Y. H.; Djurišić, A. B.; Lee, P. K. H.; Chan, W. K.; Yu, L. H.; Phillips, D. L.; Ma, A. P. Y.; Leung, F. C. C. Mechanisms of Antibacterial Activity of MgO: Non-ROS Mediated Toxicity of MgO Nanoparticles Towards *Escherichia Coli*. *Small* **2014**, *10*, 1171−1183.
(16) Hu, W.; Peng, C.; Luo, W.; Lv, M.; Li, X.; Li, D.; Huang, Q.; Fan, C. Graphene-Based Antibacterial Paper. *ACS Nano* **2010**, *4*, 4317−4323.
(17) Zou, X.; Zhang, L.; Wang, Z.; Luo, Y. Mechanisms of the Antimicrobial Activities of Graphene Materials. *J. Am. Chem. Soc.* **2016**, *138*, 2064−2077.
(18) Jayaprakash, N.; Vijaya, J. J.; Kaviyarasu, K.; Kombaiah, K.; Kennedy, L. J.; Ramalingam, R. J.; Munusamy, M. A.; Al-Lohedan, H. A. Green Synthesis of Ag Nanoparticles Using Tamarind Fruit Extract for the Antibacterial Studies. *J. Photochem. Photobiol. B* **2017**, *169*, 178−185.
(19) Biao, L.; Tan, S.; Wang, Y.; Guo, X.; Fu, Y.; Xu, F.; Zu, Y.; Liu, Z. Synthesis, Characterization and Antibacterial Study on the Chitosan-Functionalized Ag Nanoparticles. *Mater. Sci. Eng. C* **2017**, *76*, 73−80.
(20) Mirzajani, F.; Ghassempour, A.; Aliahmadi, A.; Esmaeili, M. A. Antibacterial Effect of Silver Nanoparticles on *Staphylococcus Aureus*. *Res. Microbiol.* **2011**, *162*, 542−549.
(21) Huang, X.; Qi, X.; Boey, F.; Zhang, H. Graphene-Based Composites. *Chem. Soc. Rev.* **2012**, *41*, 666−686.
(22) He, H.; Klinowski, J.; Forster, M.; Lerf, A. A New Structural Model for Graphite Oxide. *Chem. Phys. Lett.* **1998**, *287*, 53−56.
(23) Farid, M. U.; Jeong, S.; Seo, D. H.; Ahmed, R.; Lau, C.; Gali, N. K.; Ning, Z.; An, A. K. Mechanistic Insight into the in Vitro Toxicity of Graphene Oxide against Biofilm Forming Bacteria Using Laser-Induced Breakdown Spectroscopy. *Nanoscale* **2018**, *10*, 4475−4487.
(24) Liu, S.; Zeng, T. H.; Hofmann, M.; Burcombe, E.; Wei, J.; Jiang, R.; Kong, J.; Chen, Y. Antibacterial Activity of Graphite, Graphite Oxide, Graphene Oxide, and Reduced Graphene Oxide: Membrane and Oxidative Stress. *ACS Nano* **2011**, *5*, 6971−6980.
(25) Geim, A. K. Graphene: Status and Prospects. *Science* **2009**, *324*, 1530−1534.
(26) Chen, X.; Wu, G.; Jiang, Y.; Wang, Y.; Chen, X. Graphene and Graphene-Based Nanomaterials: The Promising Materials for Bright Future of Electroanalytical Chemistry. *Analyst* **2011**, *136*, 4631.
(27) Huang, X.; Yin, Z.; Wu, S.; Qi, X.; He, Q.; Zhang, Q.; Yan, Q.; Boey, F.; Zhang, H. Graphene-Based Materials: Synthesis, Characterization, Properties, and Applications. *Small* **2011**, *7*, 1876−1902.
(28) Wang, Y.; Jaiswal, M.; Lin, M.; Saha, S.; Özyilmaz, B.; Loh, K. P. Electronic Properties of Nanodiamond Decorated Graphene. *ACS Nano* **2012**, *6*, 1018−1025.
(29) Inagaki, M.; Kang, F. Graphene Derivatives: Graphane, Fluorographene, Graphene Oxide, Graphyne and Graphdiyne. *J. Mater. Chem. A* **2014**, *2*, 13193−13206.
(30) Yang, K.; Zhang, S.; Zhang, G.; Sun, X.; Lee, S.-T.; Liu, Z. Graphene in Mice: Ultrahigh In Vivo Tumor Uptake and Efficient Photothermal Therapy. *Nano Lett.* **2010**, *10*, 3318−3323.
(31) Brodie, B. C. Sur le poids atomique du graphite. *Ann. Chim. Phys.* **1860**, *59*, 466−472.
(32) Qiu, J.; Wang, D.; Geng, H.; Guo, J.; Qian, S.; Liu, X. How Oxygen-Containing Groups on Graphene Influence the Antibacterial Behaviors. *Adv. Mater. Interfaces* **2017**, *4*, No. 1700228.
(33) Staudenmaier, L. Verfahren zur Darstellung der Graphitsäure. *Ber. Dtsch. Chem. Ges.* **1898**, *31*, 1481−1487.
(34) Chua, C. K.; Sofer, Z.; Pumera, M. Graphite Oxides: Effects of Permanganate and Chlorate Oxidants on the Oxygen Composition. *Chem. Eur. J.* **2012**, *18*, 13453−13459.
(35) Hummers, W. S.; Offeman, R. E. Preparation of Graphitic Oxide. *J. Am. Chem. Soc.* **1958**, *80*, 1339.
(36) Lavin-Lopez, M. P.; Valverde, J. L.; Sanchez-Silva, L.; Romero, A. Influence of the Total Gas Flow at Different Reaction Times for CVD-Graphene Synthesis on Polycrystalline Nickel. *J. Nanomater.* **2016**, *2016*, 1−9.
(37) Yuan, Y.; Wu, H.; Lu, H.; Zheng, Y.; Ying, J. Y.; Zhang, Y. ZIF Nano-Dagger Coated Gauze for Antibiotic-Free Wound Dressing. *Chem. Commun.* **2019**, *55*, 699−702.
(38) Lee, T. H.; Yen, C. T.; Hsu, S. Preparation of Polyurethane-Graphene Nanocomposite and Evaluation of Neurovascular Regeneration. *ACS Biomater. Sci. Eng.* **2020**, *6*, 597−609.
(39) Palmieri, V.; Bugli, F.; Lauriola, M. C.; Cacaci, M.; Torelli, R.; Ciasca, G.; Conti, C.; Sanguinetti, M.; Papi, M.; Spirito, M. D. Bacteria Meet Graphene: Modulation of Graphene Oxide Nano-Sheets Interaction with Human Pathogens for an Effective Antimicrobial Therapy. *ACS Biomater. Sci. Eng.* **2017**, *3*, 619−627.
(40) Qi, Z.; Bharate, P.; Lai, C.-H.; Ziem, B.; Böttcher, C.; Schulz, A.; Beckert, F.; Hatting, B.; Mülhaupt, R.; Seeberger, P. H.; Haag, R. Multivalency at Interfaces: Supramolecular Carbohydrate-Functionalized Graphene Derivatives for Bacterial Capture, Release, and Disinfection. *Nano Lett.* **2015**, *15*, 6051−6057.
(41) Akhavan, O.; Ghaderi, E. Toxicity of Graphene and Graphene Oxide Nanowalls Against Bacteria. *ACS Nano* **2010**, *4*, 5731−5736.
(42) Pandit, S.; Cao, Z.; Mokkapati, V. R. S. S.; Celauro, E.; Yurgens, A.; Lovmar, M.; Westerlund, F.; Sun, J.; Mijakovic, I. Vertically Aligned Graphene Coating Is Bactericidal and Prevents the Formation of Bacterial Biofilms. *Adv. Mater. Interfaces* **2018**, *5*, No. 1701331.
(43) Smith, S. C.; Rodrigues, D. F. Carbon-Based Nanomaterials for Removal of Chemical and Biological Contaminants from Water: A Review of Mechanisms and Applications. *Carbon* **2015**, *91*, 122−143.
(44) Li, R.; Mansukhani, N. D.; Guiney, L. M.; Ji, Z.; Zhao, Y.; Chang, C. H.; French, C. T.; Miller, J. F.; Hersam, M. C.; Nel, A. E.; Xia, T. Identification and Optimization of Carbon Radicals on Hydrated Graphene Oxide for Ubiquitous Antibacterial Coatings. *ACS Nano* **2016**, *10*, 10966−10980.
(45) Karahan, H. E.; Wiraja, C.; Xu, C.; Wei, J.; Wang, Y.; Wang, L.; Liu, F.; Chen, Y. Graphene materials in antimicrobial nanomedicine: current status and future perspectives. *Adv. Healthcare Mater.* **2018**, *7*, No. 1701406.
(46) Gusev, A.; Zakharova, O.; Muratov, D. S.; Vorobeva, N. S.; Sarker, M.; Rybkin, I.; Bratashov, D.; Kolesnikov, E.; Lapanje, A.; Kuznetsov, D. V.; Sinitskii, A. Medium-Dependent Antibacterial Properties and Bacterial Filtration Ability of Reduced Graphene Oxide. *Nanomaterials* **2019**, *9*, 1454.
(47) Nazari, A. Preparation of Electroconductive, Antibacterial, Photoactive Cotton Fabric Through Green Synthesis of ZnO/Reduced Graphene Oxide Nanocomposite. *Fibers Polym.* **2019**, *20*, 2618−2624.
(48) Whang, M.; Kim, J. Synthetic Hydrogels with Stiffness Gradients for Durotaxis Study and Tissue Engineering Scaffolds. *Tissue. Eng. Regen. Med.* **2016**, *13*, 126−139.
(49) Dai, X.; Liu, J.; Zheng, H.; Wichmann, J.; Hopfner, U.; Sudhop, S.; Prein, C.; Shen, Y.; Machens, H. G.; Schilling, A. F. Nano-Formulated Curcumin Accelerates Acute Wound Healing through Dkk-1-Mediated Fibroblast Mobilization and MCP-1-Mediated Anti-Inflammation. *NPG Asia Mater.* **2017**, *9*, e368.
(50) Li, L.; Mendis, N.; Trigui, H.; Oliver, J. D.; Faucher, S. P. The Importance of the Viable but Non-Culturable State in Human Bacterial Pathogens. *Front. Microbiol.* **2014**, *5*, No. 258.

https://dx.doi.org/10.1021/acsbiomaterials.0c01598
ACS Biomater. Sci. Eng. 2021, 7, 752−763

(51) Sharifi-Rad, J.; Hoseini-Alfatemi, S.; Sharifi-Rad, M.; Sharifi-Rad, M.; Iriti, M.; Sharifi-Rad, M.; Sharifi-Rad, R.; Raeisi, S. Phytochemical Compositions and Biological Activities of Essential Oil from Xanthium Strumarium L. *Molecules* **2015**, *20*, 7034−7047.
(52) Lopes, E.; Piçarra, S.; Almeida, P. L.; Lencastre de H, M.; Aires-de-Sousa, M. Bactericidal efficacy of molybdenum oxide nanoparticles against antimicrobial-resistant pathogens. *J. Med. Microbiol.* **2018**, *67*, 1042−1046.
(53) Hayat, S.; Muzammil, S.; Rasool, M. H.; Nisar, Z.; Hussain, S. Z.; Sabri, A. N.; Jamil, S. In Vitro Antibiofilm and Anti-Adhesion Effects of Magnesium Oxide Nanoparticles against Antibiotic Resistant Bacteria: Antibiofilm Potential of MgO NPs. *Microbiol. Immunol.* **2018**, *62*, 211−220.
(54) Iram, S.; Akbar Khan, J.; Aman, N.; Nadhman, A.; Zulfiqar, Z.; Arfat Yameen, M. Enhancing the Anti-Enterococci Activity of Different Antibiotics by Combining With Metal Oxide Nanoparticles. *Jundishapur J. Microbiol.* **2016**, *9*, No. e31302.
(55) Ali, Z.; Raj, B.; Vishwas, M.; Athhar, M. A. Synthesis, Characterization and Antimicrobial Activity of Ce Doped TiO2 Nanoparticles. *Int. J. Curr. Microbiol. App. Sci.* **2016**, *5*, 705−712.

https://dx.doi.org/10.1021/acsbiomaterials.0c01598
ACS Biomater. Sci. Eng. 2021, 7, 752−763